NANO LETTERS

Letter

pubs.acs.org/NanoLett

Mechanical Control of Electroresistive Switching

Yunseok Kim,*[,†,‡] Simon J. Kelly,[†,§] Anna Morozovska,[∥] Ehsan Kabiri Rahani,[⊥] Evgheni Strelcov,[†] Eugene Eliseev,[#] Stephen Jesse,[†] Michael D. Biegalski,[†] Nina Balke,[†] Nicole Benedek,[▽] Dmitri Strukov,[○] J. Aarts,[§] Inrok Hwang,[◆] Sungtaek Oh,[◆] Jin Sik Choi,[◆] Taekjib Choi,[¶] Bae Ho Park,[◆] Vivek B. Shenoy,[□] Peter Maksymovych,[†] and Sergei V. Kalinin*[,†]

[†]The Center for Nanophase Materials Sciences, Oak Ridge National Laboratory, Oak Ridge, Tennessee 37831, United States

[‡]School of Advanced Materials Science & Engineering, Sungkyunkwan University, Suwon 440-746, Republic of Korea

[§]Leiden Institute of Physics, Leiden University, Niels Bohrweg 2, 2333 CA Leiden, The Netherlands

[∥]Institute of Physics, National Academy of Science of Ukraine, 46, pr. Nauki, 03028 Kiev, Ukraine

[⊥]School of Engineering, Brown University, Providence, Rhode Island 02906, United States

[#]Institute for Problems of Materials Science, National Academy of Science of Ukraine, 3, Krjijanovskogo, 03142 Kiev, Ukraine

[▽]Materials Science and Engineering Program, The University of Texas at Austin, 1 University Station, Austin, Texas 78712, United States

[○]Department of Electrical and Computer Engineering, University of California, Santa Barbara, California 93106, United States

[◆]Division of Quantum Phases & Devices, Department of Physics, Konkuk University, Seoul 143-701, Korea

[¶]Hybrid Materials Research Center and Department of Nanotechnology and Advanced Materials Engineering, Sejong University, Seoul 143-747, Korea

[□]Department of Materials Science and Engineering, University of Pennsylvania, Philadelphia, Pennsylvania 19104, United States

S *Supporting Information*

ABSTRACT: Hysteretic metal−insulator transitions (MIT) mediated by ionic dynamics or ferroic phase transitions underpin emergent applications for nonvolatile memories and logic devices. The vast majority of applications and studies have explored the MIT coupled to the electric field or temperarture. Here, we argue that MIT coupled to ionic dynamics should be controlled by mechanical stimuli, the behavior we refer to as the piezochemical effect. We verify this effect experimentally and demonstrate that it allows both studying materials physics and enabling novel data storage technologies with mechanical writing and current-based readout.

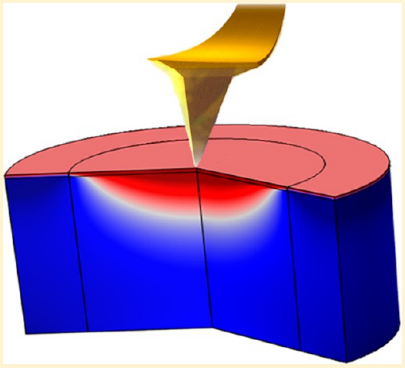

KEYWORDS: *Piezochemical effect, pressure, mechanical force, metal−insulator transition, AFM*

Metal−insulator transitions (MITs) are among the most exciting physical phenomena, both as a source of information on materials physics[1] and due to a broad gamut of novel electronic and device applications.[2−4] Of these, the hysteretic MITs controlled by external electrical or optical stimuli are of special interest as the enabling component of the information storage and logic applications that include electroresistive memories and field-effect transistors. The mechanisms of MITs are very diverse and can include intrinsic phase separation in complex oxides,[5−8] electrochemically coupled phenomena,[9−11] strain-controlled ferroic transitions,[12] and Joule-heating induced effects.[13−16] Even more complex phenomena are enabled by interfaces and thin layers, as in the ferroelectric tunneling junction.[17,18]

In virtually all cases to date, the MITs are controlled by applied electric or magnetic fields,[10,11,19] giving rise to a broad set of existent and emergent information technology applications. We note, however, that multiple classes of MITs are intrinsically coupled to strain and thus will be affected by mechanical forces. This is the case for physical MITs associated with ferroic transitions, when the mechanical force can vary the fraction of metallic high symmetry phase.[12] However, the mesoscopic scale of domains and the long-range nature of strain interactions preclude local remanent changes in

Received: April 19, 2013
Revised: July 17, 2013
Published: August 27, 2013

 © 2013 American Chemical Society

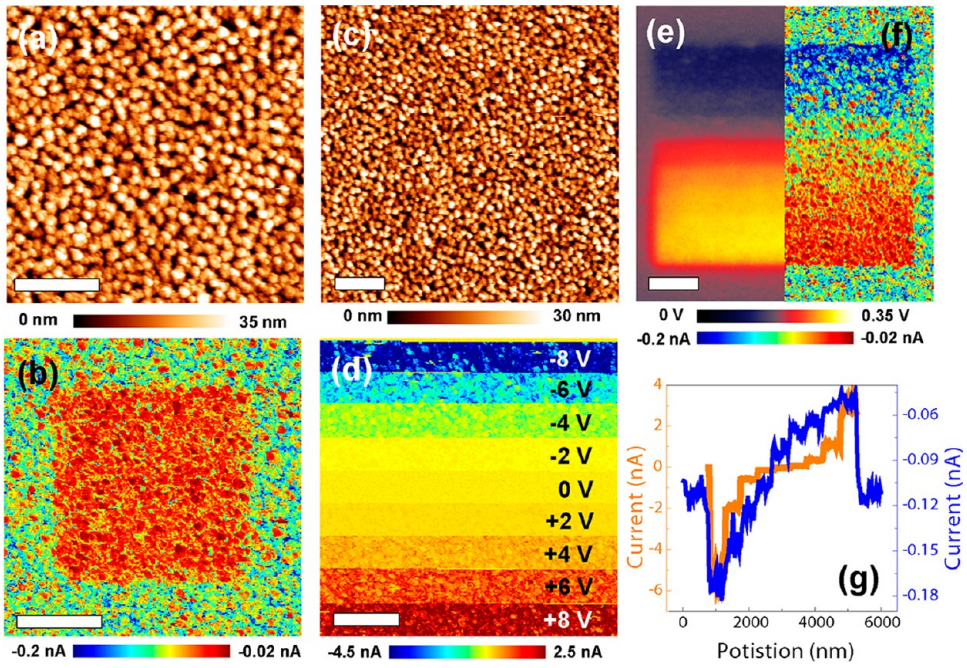

Figure 1. (a,c) Topography and (b,d,f) CAFM, and (e) KPFM images of a NiO film (a,b) after three consequtive scans over an area of 2.0 μm at 1.0 Hz with grounded (0 V) Pt/Cr coated tip, (d) during and (c,e,f) after applying bias voltages from −8 V to +8 V by Pt/Cr coated tips under the set point of 0.5 V (corresponding to 40 nN force exerted by the cantilever). CAFM images in parts b and f were taken under −2 V and set point of 0.75 V. (g) Average current line profiles from CAFM images. Orange and blue lines are taken from parts d and f, respectively. The scale bar is 1 μm.

conductance state. At the same time, ionically mediated MITs can be confined to nanometer level of several unit cells and are often hysteretic in nature, enabling broad range of applications in nonvolatile information storage and logic devices.

We note that all ionically controlled MITs are associated with molar volume changes, the behavior universally referred to as *chemical expansivity*.[20,21] This suggests, through the Le Chatelier principle, that local *strain* can be used to induce and control MITs in ionic systems, offering new opportunities for oxide electronic device fabrication and fundamental studies of MIT phenomena. On the other hand, in general, having a new way of controlling material properties (in addition to, e.g., electrical and thermal stress, and light) is always desirable and presents new opportunities for applications. Here, we explore local pressure-induced MIT in oxides and demonstrate creation of remanent conductance states.

To demonstrate this effect, we have chosen NiO as a model system in a close proximity to MITs. The MIT in NiO can be readily induced by changes of stoichiometry in NiO_{1-x}, or doping. The former can be controlled by electric bias, and consequently NiO is one of the most popular resistive switching materials.[10,11,19,22−24] In this compound, oxygen stoichiometry is expected to be strongly affected by pressure, that is, the piezochemical effect, due to the Vegard strain effects (chemical expansivity),[21,25] providing the basis for strain-controlled MITs.

To establish the presence of pressure-induced changes in surface conductance, the material surface was scanned by a grounded atomic force microsocpy (AFM) tip. As illustrated in Figure 1a,b, scanning the surface with an electrically grounded tip significantly alters its electronic conductance, that is, changing it to high-resistance state.

We further explore the bias-induced evolution in surface potential. The application of positive bias leads to positively charged surface (measured by Kelvin probe force microscopy: KPFM)[26−28] and high-resistance state (measured by conductive AFM: CAFM), as illustrated for NiO in Figure 1d−g. The surface potential behavior indicates the charge injection or electrochemical reaction near the sample surfaces.[29,30] At the same time, the observed conductance changes suggest ionically mediated electrochemical reaction during the bias-application. When the positive bias is applied to the NiO_{1-x} film surfaces, positively charged oxygen vacancies are repelled from the film surface.[19] At the same time, negatively charged oxygen ions are attracted to the film surface under positive bias. Then, NiO transforms to a stoichiometric insulating state.[31] In agreement with previous reports, different bias voltage levels control the degree of the electrochemical reactions near the surface and allow control of remanent conductance (multiple level storage).[32]

To further explore the pressure-induced MIT, the experiments were performed with high spring constant cantilevers, enabling nominal indentation forces even up to 3 μN (note that presence of capillary forces in ambient environment generally results in 50−100 nN adhesion forces). The surface was scanned by a grounded tip while increasing the tip−surface contact force from 750 nN (for set point, SP = 0.5 V) to 6 μN (for SP = 4.0 V). Subsequent KPFM and CAFM imaging has demonstrated that, on increasing the contact force, the surface potential increases and conductance decreases, as illustrated in Figure 2. In other words, pressure changes surface potential and conduction similarly to the application of positive bias to the probe at low indentation force.

To separate the contributions of normal pressure vs friction forces and wear, we performed force−distance ($F-D$) measurements on a grid of points. In these, high pressure can be applied without scanning the sample surface. The observed changes in conductance (Figure S4 in Supporting Information) are the same as during scanning. Hence, the friction effects, that

dx.doi.org/10.1021/nl401411r | *Nano Lett.* 2013, 13, 4068−4074

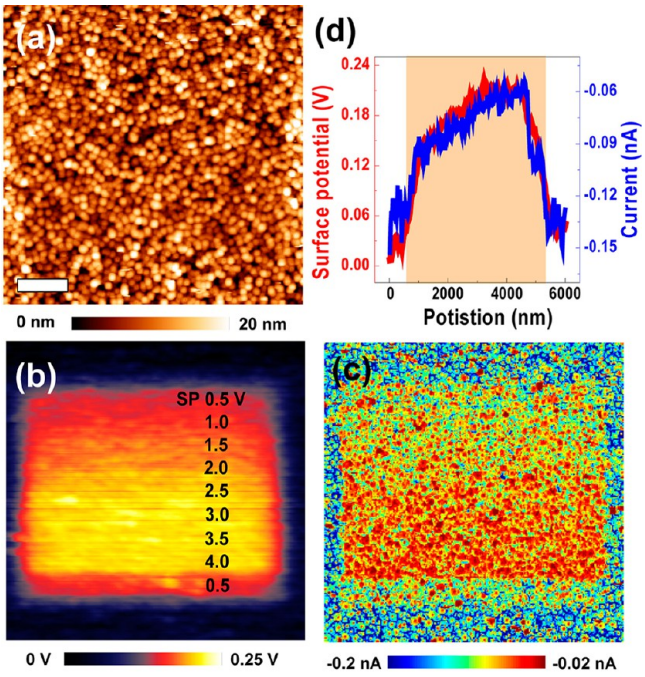

Figure 2. (a) Topography, (b) KPFM, and (c) CAFM images of a NiO film after scanning with different contact force, that is, set point SP, by diamond coated tips. (d) Line profiles from KPFM and CAFM images (parts b and c). The bright orange area presents a scanned area with different contact force. CAFM image in part c was taken under −2 V. 1.0 V of set point corresponds to about 1500 nN. The scale bar is 1 μm.

is, triboelectricity,[33−35] can be largely excluded as the origin of observed changes.

Finally, to check controllability of the pressure effect, the box patterns were formed by combination of high contact force and bias voltage. As shown in Figure 3, the surface potential and current can be well- controlled by both contact force and bias voltages. In the first case, we switched materials into low-resistance state by applying negative bias voltage and then switched back into high-resistance state by pressing the material, whereas, in the second one, we switched in high-resistance state by pressure and then switched back to the low-resistance state by bias. This provides that the pressure acts as positive bias voltage. It can only switch materials from a low to a high-resistance state; however this low-resistance state can be reversed by negative bias voltage. We further note that the pressure- and bias induced conduction variations are long-lived and can be observed to persist for at least 15 h (see Figure S6).

Pressure-induced formation of the region with decreased conduction can be attributed to several possible mechanisms. The primary interaction we consider is piezochemical coupling, in which applied pressure shifts electrochemical potential of oxygen vacancies through Vegard, flexoelectric, and deformation potential effects.[36] Due to the relatively low mobility of oxygen vacancies, thus induced changes are kinetically frozen and can be detected as remanent changes in conductance.

The magnitude of this effect can be readily estimated from chemical expansion and deformation potential theories.[37−41] The strain-induced conduction (valence) band edge shift (deformation potential) is proportional to the strain variation, $\delta u_{ij}(\mathbf{r})$, that is, $E_C(u_{ij}(\mathbf{r})) = E_{C0} + \Xi_{ij}^C u_{ij}(\mathbf{r})$, $E_V(u_{ij}(\mathbf{r})) = E_{V0} + \Xi_{ij}^V \delta u_{ij}(\mathbf{r})$, where E_C and E_V are the position of the bottom of conduction band and the top of the valence band, respectively,[42] $\Xi_{ij}^{C,V}$ is a deformation potential tensor of electrons in the conduction (C) and valence bands (V). The symmetry of the deformation potential tensors $\Xi_{ij}^{C,V}$ are rather

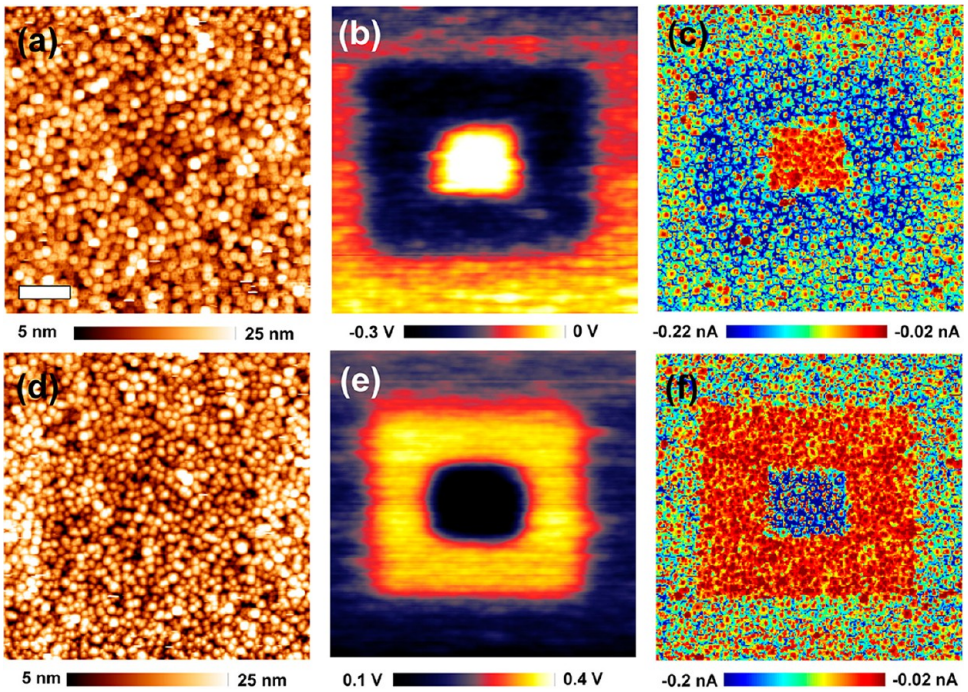

Figure 3. (a,d) Topography, (b,e) KPFM, and (c,f) CAFM images of a NiO film after box patterning by a diamond coated tip: (a−c) background box pattern: bias voltage of −6 V, inner box pattern: set point of 1.5 V, (d−f) background box pattern: set point of 1.5 V, inner box pattern: bias voltage of −6 V. CAFM images in parts c and f were taken under −2 V. 1.0 V of set point corresponds to about 1500 nN. There is slight topographic change due to application of high contact force. The scale bar is 1 μm.

dx.doi.org/10.1021/nl401411r | Nano Lett. 2013, 13, 4068−4074

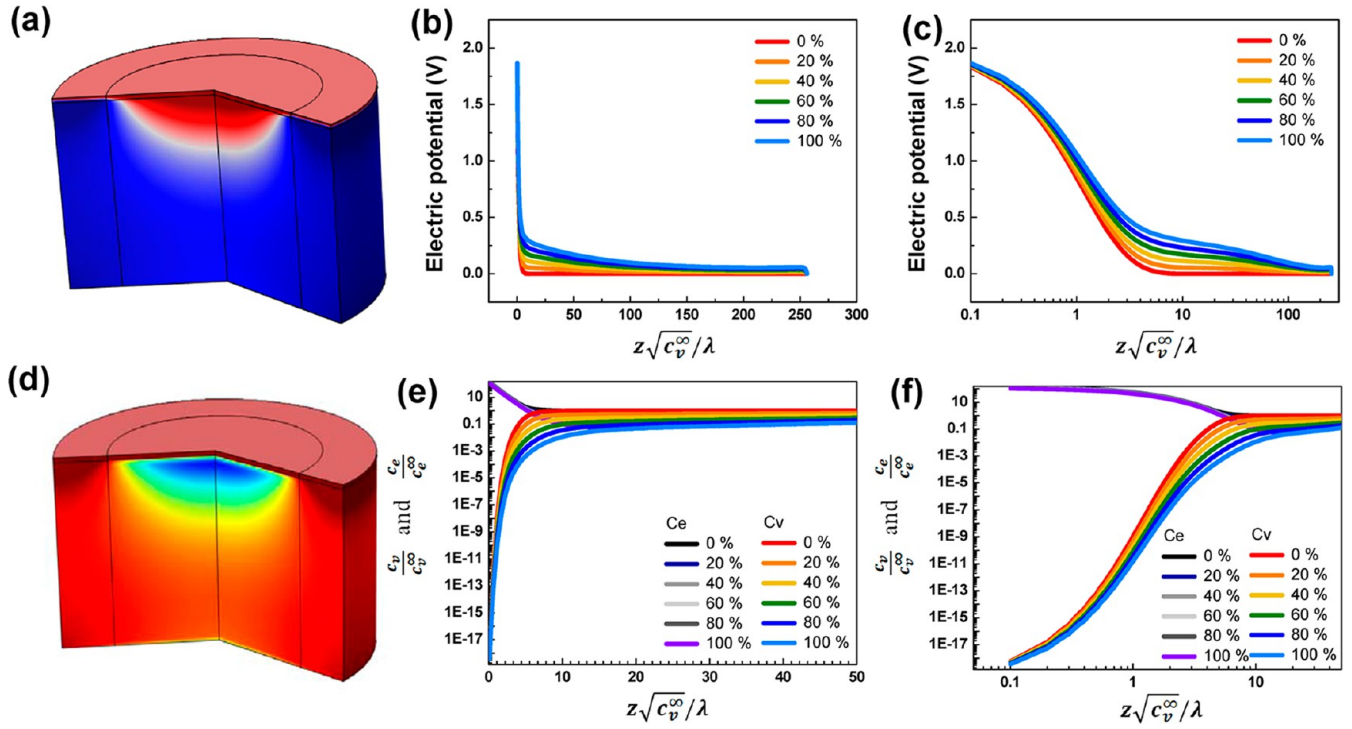

Figure 4. (a) 3D profile of the electric potential, (b) electric potential, (c) electric potential (log scale x axis), (d) 3D profile of $\log(c_e/c_e^\infty)$, (e) defect concentrationon, and (f) defect concentration (log scale x and y axes) profiles, 2.0 V bias voltage, F_{ind} = 3 μN (indentation force), c_v^∞ = 0.01, cell size = 256 $\lambda/(c_v^\infty)^{1/2}$ (λ is the Debye length).

complex but coincide with the crystal spatial symmetry at the Γ-point.[43] Here, since the spontaneous tetragonal or orthorhombic distortions are absent in the parent phase, we use the cubic parent phase approximation of the deformation potential for numerical calculations, that is, $\Xi_{ij}^{C,V} = -\Xi_d^{C,V}\delta_{ij}$ (δ_{ij} is a Kroneker symbol). Typical values of $\Xi_d^{C,V}$ are ∼5−10 eV. To determine the numerical value of deformation potential, we performed density functional theory (DFT) calculations to gauge the effect of strain on the NiO band gap (see the Methods section for technical details). DFT does not accurately describe the detailed features of the electronic structure of NiO,[44] but we expect *trends* in band gaps and band edges to be correct. Figure S7 shows that tensile strain by itself significantly lowers (by ∼0.1 eV) the calculated gap, even in the absence of stoichiometry changes.

The second contribution to pressure-induced effects is flexoelectric coupling, $\delta P_i = a_{ij}^{-1}(f_{mnjl}/2)(\partial u_{mn}/\partial x_l)$, where f_{mnjl} is the flexoelectric effect tensor. Electric field $E_i = -\partial\varphi/\partial x_i$ and electrostatic potential φ should be determined from the Poisson equation. Then, variation of the electric field related to the flexoelectric effect is written as $\delta E_j = -(\chi_{ij}^{-1}/\varepsilon_0)\delta P_i \approx -f_{mnjl}(\partial u_{mn}/\partial x_l)$, where $a_{ik}^{-1} \equiv 2\varepsilon_0\chi_{ik}$ and χ_{ij} is the related susceptibility. To estimate the electric potential variation $\delta\varphi$ caused by the electric field δE_j, we assume that all variables depend only on the distance z from the surface. For the case, $\delta E_z = -d\delta\varphi/dz$, and therefore $\delta\varphi_{flexo}(z) = -\int_{-\infty}^{z}dz'\delta E_z(z') = f_{mn33}\int_{-\infty}^{z}dz'(\partial u_{mn}/\partial z') = f_{mn33}\delta u_{mn}(z)$. Consequently, the free carrier density can be estimated in the Boltzmann approximation[36] $n = n_0\exp((\Xi_d^C\delta u_{ii} + e\delta\varphi_{flexo} + e\varphi_{ext})/k_BT)$ for free electrons, where φ_{ext} is applied an external potential, n_0 is their bulk concentrations, k_B = 1.3807 × 10^{-23} J/K, and T is the absolute temperature. The total tip-induced variation of electrochemical potential at the surface is $\delta\mu_n = \Xi_d^C\delta u_{ii} + e\delta\varphi_{flexo} + e\varphi_{ext}$ for electrons, or $\delta\mu_n \approx (\Xi_{ij}^C + ef_{ij33})s_{ijkl}\sigma_{kl} - e\varphi_{ext}$ in linear approximation of the linear Hooke law, $u_{ij} = s_{ijkl}\sigma_{kl} + ...$ (s_{ijkl} is elastic compliance).

Finally, the third component for vacancies is the Vegard term, that is, coupling between molar volume and vacancy concentration. This term yields to relations for stress $\sigma_{ij} = c_{ijkl}u_{kl}(\mathbf{r}) + \beta_{ij}^d(N_d^+(\mathbf{r}) - N_{d0}^+)$ and strain $u_{ij} = s_{ijkl}\sigma_{kl}(\mathbf{r}) - \tilde{\beta}_{ij}^d(N_d^+(\mathbf{r}) - N_{d0}^+)$, where $\tilde{\beta}_{ij}^d = s_{ijkl}\beta_{kl}^d$ are the *Vegard expansion* tensors for donors (vacancies). Consequently, equilibrium concentrations of the donors are in the Boltzmann−Planck−Nernst approximation $N_d^+ \approx N_{d0}^+\exp((\beta_{ij}^d\delta u_{ij} - ef_{ij33}\delta u_{ij} - e\varphi_{ext})/k_BT)$.[36] The total tip-induced variation of electrochemical potential for vacancies is $\delta\mu_{N_d} = \beta_{ij}^d\delta u_{ij} - ef_{ij33}\delta u_{ij} + e\varphi_{ext}$. Using the Hooke law, it can be rewritten as $\delta\mu_{N_d} = \tilde{\beta}_{ij}^d\sigma_{ij} - ef_{ij33}s_{ijkl}\sigma_{kl} + e\varphi_{ext}$.

For NiO,[45−48] we estimated diagonal component $\tilde{\beta}$ of $\tilde{\beta}_{jk}^d = \delta_{ik}\tilde{\beta}$ as ranging from −8 Å^3 to −20 Å^3 and obtained $\beta \approx$ (2−40) eV for elastic stiffnesses of c_{11} = 224 and c_{12} = 97 GPa[49] (Figure S7). The pressure induced changes in electrochemical potential for electrons and vacancies can be as high as 0.28 eV for pressures of the order of ∼3 GPa, as generated in the contact of 10 nm radius under ∼10^3 nN indentation force. These simple estimations suggest that piezochemical coupling is a fully realistic effect that should manifest for large indentation forces in materials with high ionic mobility. Note that the flexoelectric, deformation potential, and Vegard effects cannot be decoupled unambiguously.

In addition to the piezochemical effect, we note that other mechanisms can operate in a tip−surface junction.[33] These include grounded tip effect, that is, the transfer of charge between surface charges and a grounded tip after their contact and subsequent separation and can be referred as a purely electrostatic effect,[29] triboelectricitiy, which is the transfer of charge caused by friction,[33−35] and wear effect, which can

dx.doi.org/10.1021/nl401411r | Nano Lett. 2013, 13, 4068−4074

induce physical damage on the surfaces and results in surface defects (e.g., selective removal of oxygen adatoms was demonstrated by Gai and Kourtakis[50]). While the wear effect accompanies visible topographic damage, the piezochemical effect under low contact force in Figure 1a is not expected to give the significant topographic change. Thus, given the absence of visible topographic damage in Figure 1a, the wear effect can be excluded. As we discuss in the Supporting Information, all of these effects can be largely excluded based on the rate-dependent contact measurements and the sign of the change of the surface potential as a result of surface scanning with a grounded metal coated tip.[29]

Finally, to explore the effect of pressure on ionic dynamics in realistic geometries, we performed full 3D numerical simulations based on the solution of coupled system of mechanical equilibrium and Poisson equations. The pressure and potential effect on the ion and electron concentration was chosen to be

$$c_v(r,z) = c_v^{\infty} \exp\left\{\frac{\overline{V}_v}{3RT}[\sigma_r(r,z) + \sigma_\theta(r,z) + \sigma_z(r,z)]\right\} \times \exp\left\{\frac{-2F}{RT}\Delta\varphi(r,z)\right\} \quad (1)$$

$$c_e(r,z) = c_e^{\infty} \exp\left\{\frac{\overline{V}_e}{3RT}[\sigma_r(r,z) + \sigma_\theta(r,z) + \sigma_z(r,z)]\right\} \times \exp\left\{\frac{+2F}{RT}\Delta\varphi(r,z)\right\}$$

following the work by Sheldon and Shenoy.[51] Here, the first exponential term represents the effect of free volume of the carriers and ions, and the second is electrostatic potential. In eq 1, c_v^{∞} and c_e^{∞} are oxygen vacancy and extra electron concentrations in bulk, respectively, $\overline{V}_v$ and $\overline{V}_e$ are partial molar volumes for oxygen vacancy and extra electron, respectively; σ_r, σ_θ, and σ_z are the stress components, and $\Delta\varphi$ is the electric potential difference between the point (r,z) and bulk, F and R are Faraday and gas constants, respectively. The details of the material parameters chosen in this study are provided in the Supporting Information. The boundary conditions are chosen corresponding to the Hertzian[52] solution for indendation, $p(r,0) = p_0(1 - (r^2/a_c^2))^{0.5}$ $(r \le a_c)$, where $p_0 = (2E^*a_c/\pi R_i)$ in which a_c is the contact area radius and R_i is the indenter tip radius and E^* represents the effective Young's modulus calculated in terms of surface and indenter tip elastic properties.

Shown in Figure 4 are the computed distributions of the electrostatic potential and ionic concentrations in NiO, as well as corresponding depth profiles. Interestingly, the presence of mechanical stress can shift the *electrochemical* potential in the system by several hundred meV, more than sufficient to induce MIT. The range of this effect is determined by the characteristic tip size and can significantly exceed that of the electrostatic field produced by the tip. While the tip biases can be considerably higher with associated shifts in electrochemical potentials, their penetration length is of the order of Debye length for the conductive NiO. This mechanism suggests the asymmetry between metal-to-insulator and insulator-to-metal transitions, since in the insulating state the penetration depth of elastic and electric fields is comparable. Hence, these estimates suggest that pressure-induced changes in the electrochemical potential are of sufficient magnitude to induce MIT and at the same time are long-ranged (compared to stronger but short-range bias effects).

To summarize, we have predicted and experimentally observed the pressure-induced changes in conductivity of transition metal oxides presumably mediated by changes in stoichiometry, of which behavior we refer to as the piezochemical effect. This behavior is expected to be universal in transition metal oxides and can be predicted based on the deformation potential, flexoelectric effect, and chemical expansivity.

The piezochemical effect allows mechanical manipulation of local resistivity down to the nanometer level. This provides insight into the pressure-controlled physics of transition metal oxides and also allows development of new generation of information storage devices with mechanical recording and current-based readout. For example, one might use piezoelectric layers coupled with electroresistive material and the pressure-controlled electroresistance can be feasibly mediated through ferroelectric domains.[53] In the context of the most practical application of electroresistive effect—in passive crossbar memories—a potential advantage of using mechanical stress (e.g., overheating) is a possibility for confining stress and thus has less parasitic coupling between neighboring memory cells.

In addition, the "voltage−time" dilemma of the electroresistive (memristive) devices arises from the fact that, to have large retention-to-write-time ratio, one either has to apply very high electric field and/or to heat it up to high temperatures. The problem is that both approaches are detrimental to the device endurance and variations. Enforcing nonlinear ion dynamics with mechanical stress may help to alleviate this issue. Furthermore, nonlinear modulation of the ion/defect mobilities could be available in many other applications, for example, to increase power density in fuel cells and to understand local strains, associated with electroforming, can be coupled to the electrochemistry.

Methods. *Materials.* A 50 nm thick polycrystalline NiO_{1-x} thin film was prepared by the sputtering method on $SrRuO_3$/$SrTiO_3$ substrate (substrate temperature: 500 °C, working pressure of Ar + O_2 mixture gas: 1.5 mTorr, O_2 ratio: 7%).[23]

Measurements. Ambient AFM studies were performed with a commercial system (Asylum Research Cypher) additionally equipped with a current amplifier (FEMTO DLPCA-200). CAFM and KPFM were carried out with applying biases to Pt/Cr (Budget sensors Multi75E-G) and boron-doped diamond (NT-NDT DCP20) coated tips. The spring constant of each cantilever was obtained from force−distance measurements and subsequent thermal tuning methods. The spring constants of Pt/Cr and diamond coated cantilever is 1.6 N/m and 70 N/m, respectively. Each 1.0 V of set point for Pt/Cr and diamond coated cantilever corresponds to about 80 nN and 1500 nN, respectively.

DFT. DFT calculations were performed within the local spin density approximation with projector augmented wave potentials, as implemented in VASP. We used a 4 × 4 × 4 k-point mesh (increased to 8 × 8 × 8 for calculations of the density of states), a 500 eV plane wave cutoff and set $U_{eff} = U - J = 7.05$ eV, as determined by Anisimov and co-workers.[54] The antiferromagentic ordering was along the [111] direction, which reduces the symmetry of the $Fm\bar{3}m$ rock salt structure to $R\bar{3}m$. The rhombohedral distortion induced by the magnetic ordering is negligible in NiO, and so we only performed calculations on cubic cells. The lattice constant (4.10 Å),

dx.doi.org/10.1021/nl401411r | Nano Lett. 2013, 13, 4068−4074

magnetic moment on Ni (1.75 μ_B), and band gap (3.97 eV) were in good agreement with previous theoretical calculations[55−57] and with the experiment.[58−61] For the strain calculations, we applied C_{11} strains of up to 4% (tensile and compressive) of the equilibrium theoretical lattice constant.

Finite Element Modeling.[52] The combined system of mechanical equilibrium equations and Poisson equation with the for charge carries were solved using finite element methods as described in ref 51. The material parameters can be found in the Supporting Information.

■ ASSOCIATED CONTENT

Supporting Information

Experimental results, theory of piezochemical effect, Figures S1−S9, Table 1. This material is available free of charge via the Internet at http://pubs.acs.org.

■ AUTHOR INFORMATION

Corresponding Authors

*E-mail: yunseokkim@skku.edu.
*E-mail: sergei2@ornl.gov.

Notes

The authors declare no competing financial interest.

■ ACKNOWLEDGMENTS

Research was supported (S.V.K., Y.K., P.M.) by the U.S. Department of Energy, Basic Energy Sciences, Materials Sciences and Engineering Division. A portion of this research was conducted as user project at the Center for Nanophase Materials Sciences (support for S.J., M.D.B., N.B.), which is sponsored at Oak Ridge National Laboratory by the Scientific User Facilities Division, Office of Basic Energy Sciences, U.S. Department of Energy. This work was also supported by (I.H., S.O., J.S.C., B.H.P.) the National Research Foundation of Korea (NRF) grants funded by the Korea government (MSIP) (No. 2013R1A3A2042120), (T.C.) Basic Science Research Program through the NRF funded by the Korea MEST (Grant No. 2011-0025607), and (S.J.K., J.A.) NanoNed, a national nanotechnology program coordinated by the Dutch Ministry of Economic Affairs. V.B.S. gratefully acknowledges the support of the Army Research Office through Contract W911NF-11-1-0171.

■ REFERENCES

(1) Imada, M.; Fujimori, A.; Tokura, Y. *Rev. Mod. Phys.* **1998**, *70* (4), 1039−1263.
(2) Hwang, H. Y.; Iwasa, Y.; Kawasaki, M.; Keimer, B.; Nagaosa, N.; Tokura, Y. *Nat. Mater.* **2012**, *11*, 103−113.
(3) Mathews, S.; Ramesh, R.; Venkatesan, T.; Benedetto, J. *Science* **1997**, *276* (5310), 238−240.
(4) Mannhart, J.; Schlom, D. G. *Science* **2010**, *327* (5973), 1607−1611.
(5) Dagotto, E.; Hotta, T.; Moreo, A. *Phys. Rep.: Rev. Sec. Phys. Lett.* **2001**, *344* (1−3), 1−153.
(6) Fath, M.; Freisem, S.; Menovsky, A. A.; Tomioka, Y.; Aarts, J.; Mydosh, J. A. *Science* **1999**, *285* (5433), 1540−1542.
(7) Tokura, Y. *Rep. Prog. Phys.* **2006**, *69* (3), 797−851.
(8) Dagotto, E. *Science* **2005**, *309* (5732), 257−262.
(9) Szot, K.; Rogala, M.; Speier, W.; Klusek, Z.; Besmehn, A.; Waser, R. *Nanotechnology* **2011**, *22* (25), 254001.
(10) Waser, R.; Dittmann, R.; Staikov, G.; Szot, K. *Adv. Mater.* **2009**, *21* (25−26), 2632.
(11) Sawa, A. *Mater. Today* **2008**, *11* (6), 28−36.
(12) Tselev, A.; Strelcov, E.; Luk'yanchuk, I. A.; Budai, J. D.; Tischler, J. Z.; Ivanov, I. N.; Jones, K.; Proksch, R.; Kalinin, S. V.; Kolmakov, A. *Nano Lett.* **2010**, *10* (6), 2003−2011.
(13) Alexandrov, A. S.; Bratkovsky, A. M.; Bridle, B.; Savel'ev, S. E.; Strukov, D. B.; Williams, R. S. *Appl. Phys. Lett.* **2011**, *99* (20), 202104.
(14) Chang, S. H.; Chae, S. C.; Lee, S. B.; Liu, C.; Noh, T. W.; Lee, J. S.; Kahng, B.; Jang, J. H.; Kim, M. Y.; Kim, D. W.; Jung, C. U. *Appl. Phys. Lett.* **2008**, *92* (18), 183507.
(15) Ielmini, D. *Phys. Rev. B* **2008**, *78* (3), 035308.
(16) Kaplan, T.; Adler, D. *Appl. Phys. Lett.* **1971**, *19* (10), 418.
(17) Maksymovych, P.; Jesse, S.; Yu, P.; Ramesh, R.; Baddorf, A. P.; Kalinin, S. V. *Science* **2009**, *324* (5933), 1421−1425.
(18) Garcia, V.; Fusil, S.; Bouzehouane, K.; Enouz-Vedrenne, S.; Mathur, N. D.; Barthelemy, A.; Bibes, M. *Nature* **2009**, *460* (7251), 81−84.
(19) Kim, K. M.; Jeong, D. S.; Hwang, C. S. *Nanotechnology* **2011**, *22* (25), 254002.
(20) Chen, X. Y.; Yu, J. S.; Adler, S. B. *Chem. Mater.* **2005**, *17* (17), 4537−4546.
(21) Adler, S. B. *J. Am. Ceram. Soc.* **2001**, *84* (9), 2117−2119.
(22) Waser, R.; Aono, M. *Nat. Mater.* **2007**, *6* (11), 833−840.
(23) Choi, J. S.; Kim, J. S.; Hwang, I. R.; Hong, S. H.; Jeon, S. H.; Kang, S. O.; Park, B. H.; Kim, D. C.; Lee, M. J.; Seo, S. *Appl. Phys. Lett.* **2009**, *95* (2), 022109.
(24) Oka, K.; Yanagida, T.; Nagashima, K.; Kawai, T.; Kim, J. S.; Park, B. H. *J. Am. Chem. Soc.* **2010**, *132* (19), 6634.
(25) Tsipis, E. V.; Kharton, V. V. *J. Solid State Electrochem.* **2011**, *15* (5), 1007−1040.
(26) Nonnenmacher, M.; Oboyle, M. P.; Wickramasinghe, H. K. *Appl. Phys. Lett.* **1991**, *58* (25), 2921−2923.
(27) Melitz, W.; Shen, J.; Kummel, A. C.; Lee, S. *Surf. Sci. Rep.* **2011**, *66* (1), 1−27.
(28) Sadewasser, S.; Glatzel, T., Eds. *Kelvin Probe Force Microscopy*; Springer Science and Business Media: New York, 2011.
(29) Kim, Y.; Bae, C.; Ryu, K.; Ko, H.; Kim, Y. K.; Hong, S.; Shin, H. *Appl. Phys. Lett.* **2009**, *94* (3), 032907.
(30) Kim, H.; Hong, S.; Kim, D.-W. *Appl. Phys. Lett.* **2012**, *100* (2), 022901.
(31) Lee, M. H.; Kim, K. M.; Song, S. J.; Rha, S. H.; Seok, J. Y.; Jung, J. S.; Kim, G. H.; Yoon, J. H.; Hwang, C. S. *Appl. Phys. A: Mater.* **2011**, *102* (4), 827−834.
(32) Pellegrino, L.; Manca, N.; Kanki, T.; Tanaka, H.; Biasotti, M.; Bellingeri, E.; Siri, A. S.; Marré, D. *Adv. Mater.* **2012**, *24* (21), 2929−2934.
(33) Baytekin, H. T.; Patashinski, A. Z.; Branicki, M.; Baytekin, B.; Soh, S.; Grzybowski, B. A. *Science* **2011**, *333* (6040), 308−312.
(34) Fukada, E.; Fowler, J. F. *Nature* **1958**, *181* (4610), 693−694.
(35) Henniker, J. *Nature* **1962**, *196* (4853), 474.
(36) Morozovska, A. N.; Eliseev, E. A.; Tagantsev, A. K.; Bravina, S. L.; Chen, L. Q.; Kalinin, S. V. *Phys. Rev. B* **2011**, *83* (19), 195313.
(37) Herring, C.; Vogt, E. *Phys. Rev.* **1956**, *101* (3), 944−961.
(38) Liu, J. F.; Cannon, D. D.; Wada, K.; Ishikawa, Y.; Danielson, D. T.; Jongthammanurak, S.; Michel, J.; Kimerling, L. C. *Phys. Rev. B* **2004**, *70* (15), 155309.
(39) Ziman, J. M. *Principles of the Theory of Solids*; Cambridge University Press: New York, 1972.
(40) Lim, J. S.; Yang, X.; Nishida, T.; Thompson, S. E. *Appl. Phys. Lett.* **2006**, *89* (7), 073509.
(41) Nolte, D. D.; Walukiewicz, W.; Haller, E. E. *Phys. Rev. Lett.* **1987**, *59* (4), 501−504.
(42) Ashcroft, N. W.; Mermin, N. D. *Solid State Physics*; Holt, Rinehart and Winston: New York, 1976; p 826.
(43) Sun, Y.; Thompson, S. E.; Nishida, T. *J. Appl. Phys.* **2007**, *101* (10), 104503.
(44) Kunes, J.; Anisimov, V. I.; Skornyakov, S. L.; Lukoyanov, A. V.; Vollhardt, D. *Phys. Rev. Lett.* **2007**, *99* (15), 156404.
(45) Bhatt, S. J.; Merchant, H. D. *J. Am. Ceram. Soc.* **1969**, *52* (8), 452.

(46) Mrowec, S.; Grzesik, Z. *J. Phys. Chem. Solids* **2004**, *65* (10), 1651−1657.
(47) Fievet, F.; Germi, P.; Bergevin, F. D.; Figlarz, M. *J. Appl. Crystallogr.* **1979**, *12* (Aug), 387−394.
(48) Freedman, D. A.; Roundy, D.; Arias, T. A. *Phys. Rev. B* **2009**, *80* (6), 064108.
(49) Towler, M. D.; Allan, N. L.; Harrison, N. M.; Saunders, V. R.; Mackrodt, W. C.; Apra, E. *Phys. Rev. B* **1994**, *50* (8), 5041−5054.
(50) Gai, P. L.; Kourtakis, K. *Science* **1995**, *267* (5198), 661−663.
(51) Sheldon, B. W.; Shenoy, V. B. *Phys. Rev. Lett.* **2011**, *106* (21), 216104.
(52) Popov, V. L. Rigorous Treatment of Contact Problems − Hertzian Contact. In *Contact Mechanics and Friction: Physical Principles and Applications*, Springer: New York, 2010; pp 55−70.
(53) Lu, H.; Bark, C. W.; de los Ojos, D. E.; Alcala, J.; Eom, C. B.; Catalan, G.; Gruverman, A. *Science* **2012**, *336* (6077), 59−61.
(54) Anisimov, V. I.; Zaanen, J.; Andersen, O. K. *Phys. Rev. B* **1991**, *44* (3), 943−954.
(55) Cococcioni, M.; de Gironcoli, S. *Phys. Rev. B* **2005**, *71* (3), 035105.
(56) Novak, P.; Kunes, J.; Chaput, L.; Pickett, W. E. *Phys. Status Solidi B* **2006**, *243* (3), 563−572.
(57) Tran, F.; Blaha, P.; Schwarz, K.; Novak, P. *Phys. Rev. B* **2006**, *74* (15), 155108.
(58) Bartel, L. C.; Morosin, B. *Phys. Rev. B* **1971**, *3* (3), 1039.
(59) Cheetham, A. K.; Hope, D. A. O. *Phys. Rev. B* **1983**, *27* (11), 6964−6967.
(60) Hufner, S.; Osterwalder, J.; Riesterer, T.; Hulliger, F. *Solid State Commun.* **1984**, *52* (9), 793−796.
(61) Sawatzky, G. A.; Allen, J. W. *Phys. Rev. Lett.* **1984**, *53* (24), 2339−2342.

■ NOTE ADDED AFTER ASAP PUBLICATION

The Acknowledgments have been updated. The revised version re-posted on August 30, 2013.